Geoderma 428 (2022) 116086

Contents lists available at ScienceDirect

Geoderma

journal homepage: www.elsevier.com/locate/geoderma

Digital soil mapping of peatland using airborne radiometric data and supervised machine learning – Implication for the assessment of carbon stock

Dave O'Leary, Colin Brown, Eve Daly *

Hy-Res Research Group, Earth and Ocean Sciences and Ryan Institute, College of Science and Engineering, National University of Ireland, Galway, Galway H91 TK33, Ireland

ARTICLE INFO

Handling Editor: Budiman Minasny

Keywords:
Peatland restoration
Neural networks
Airborne geophysics

ABSTRACT

Peatlands account for approx. 4.23 million km^2 of the land surface of Earth and between 5 % and 20 % of the global soil carbon stock, however much uncertainty exists. The release of carbon from modified peatlands is significant and affects the global carbon balance. The importance of conservation and rehabilitation of peatlands is clear. Global estimates currently use national scale mapping strategies that vary depending on available resources and national interest. The most up-to-date methods rely on satellite remote sensing data, which detect peat based on a multiband spectral signature, or reflected radar backscatter. However, satellite data may not be capable of detecting peat under landcover such as pasture or forest. Airborne geophysical surveys provide relevant subsurface information to update or redefine peatland extent maps at a national scale. Radiometric surveys, which measure the naturally occurring geologically sourced potassium, uranium, and thorium, offer the largest potential. Modelling of gamma ray attenuation shows that peat has a distinctive attenuation signature, due to its low bulk density, when considering all recorded radiometric data. This study exploits this signature by combining airborne radiometric data in a machine learning framework and training an artificial neural network to detect those data which have been acquired over previously mapped peatlands. A ~95 % predictability is achieved. The trained neural network can be then used to predict the extent of all peatlands within a region, including forested and agriculturally modified peatlands, and an updated peatland map can be produced. This methodology has implications for global carbon stock assessment and rehabilitation projects where similar datasets exist or are planned, by updating the extent and boundary positions of current peatlands and uncovering previously unknown peatlands under forestry or grasslands.

1. Introduction

Peatlands provide a range of ecosystem services such as water regulation, biodiversity, and climate regulation (Grand-Clement et al., 2013; Kareksela et al., 2015). They occur globally (Fig. 1) in the humid tropics (e.g., Southeast Asia) and cool temperate regions (e.g., northern Europe) (Dargie et al., 2017; Tanneberger et al., 2017; Xu et al., 2018). Peatlands are estimated to account for approximately 4.23 million km^2 (or 2.84 %) of the global land area (Xu et al., 2018) and contain between 5 % and 20 % of the global soil carbon (C) stock (Treat et al., 2019). The release of C from drained peatlands is significant and affects the global C balance (Evans et al., 2021; Kareksela et al., 2015; Qiu et al., 2020; Yu et al., 2011). The importance of conservation and restoration of peatlands in reducing greenhouse gas emissions can be seen with the creation of the Global Peatlands Initiative (GPI, 2016), recent reports (Searchinger et al., 2022) and the ambitious 55 % reduction in emissions outlined in the European Union (EU) 2030 climate and energy framework (EU, 2020). However, there are considerable uncertainties at all scales (local to global) on peatland extent and volume (Xu et al., 2018) and new tools are required to update existing peatland databases (Minasny et al., 2019; Monteverde et al., 2022).

At the global scale, peatland maps are created by combining the Harmonized World Soil Database (HSWD) with regional and nationally available soil maps (Xu et al., 2018; Yu et al., 2010). A review paper (Minasny et al., 2019) outlines 12 national scale peat mapping attempts (Brazil, Indonesia, Scotland, Ireland, Canada etc), ranging from

* Corresponding author.
E-mail address: eve.daly@universityofgalway.ie (E. Daly).

https://doi.org/10.1016/j.geoderma.2022.116086
Received 9 May 2022; Received in revised form 2 August 2022; Accepted 3 August 2022
Available online 20 September 2022

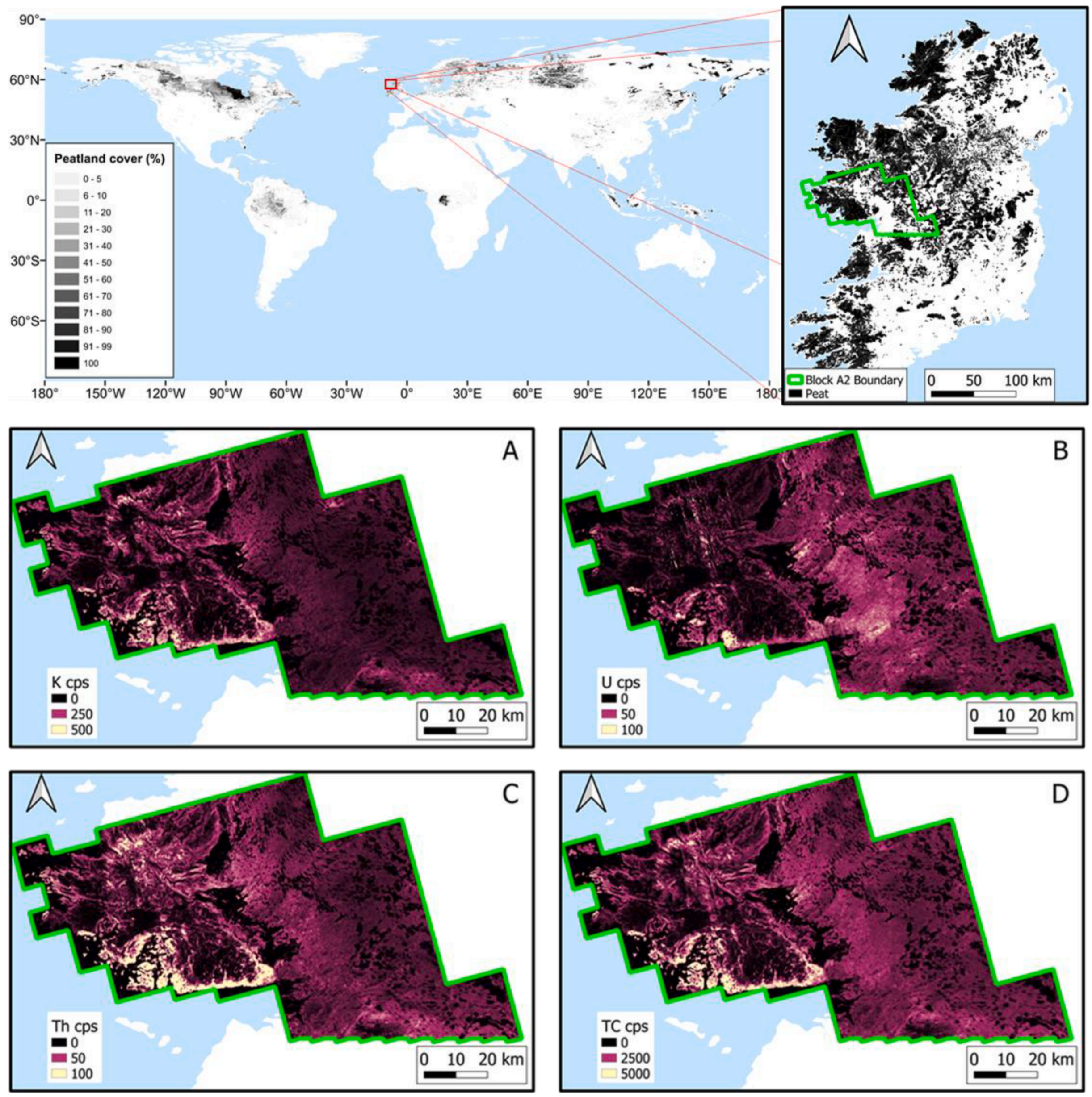

Fig. 1. PEATMAP Global peatland area estimation (Xu et al., 2018), creative common (Top Left), PEATMAP of Ireland, with study location boundary of Tellus Block A2, green boundary (Top Right). Tellus Block A2 Radiometric data (Bottom). A) Potassium cps. B) Uranium cps. C) Thorium cps. D) Total Counts cps.

traditional methods to modern digital soil mapping techniques (McBratney et al., 2003; Zhang et al., 2017). The inconsistent techniques, and the uncertainties for each technique, used in national scale soil mapping projects translates to global uncertainty of peatland extent (Xu et al., 2018). Countries with access to remotely sensed satellite and geophysical data can provide more accurate national peatland maps, and the inclusion of these data should be encouraged (Minasny et al., 2019). Additionally increases in peatland map resolutions are needed to include previously unmapped peat in national inventories (Connolly and Holden 2009).

Optical satellite data are often used as part of national mapping projects (Aitkenhead, 2017). Their high spatial resolutions (10–30 m) measure the surface reflectance for several bands of visible and near-visible electromagnetic energy. Often, individual optical images are combined into land cover maps, an example is CORINE 2018 produced at a scale of 25 ha (ha) (CORINE, 2018) to detect peatlands (Aune-Lundberg and Strand, 2021; Wijedasa et al., 2012). Synthetic Aperture Radar (SAR) satellite data measures the strength of a returning radar signal and are sensitive to moisture to depths of ~ 10 cm and spatial resolutions of ~ 10 m (Wang and Qu, 2009). These data have been used successfully to delineate peatlands (Merchant et al., 2017; Novresiandi and Nagasawa, 2017). SAR data are unaffected by cloud coverage, however they are sensitive to local meteorological conditions such as rainfall (Hird et al., 2017), which affects soil moisture, making global mapping difficult without significant ground calibration. Optical and SAR remote sensing techniques sample the landcover and the very near surface respectively and so may not detect peat soils modified by agriculture or forestry (Gatis et al., 2019), which are significant contributors to C stock assessment (Donlan et al., 2016; Wilson et al., 2016).

National scale geophysical surveys appear to provide the most accurate estimates of peatland area, with the electromagnetic (Boaga et al., 2020; Siemon et al., 2020) and radiometric (Airo et al., 2014; Berglund and Berglund, 2010) methods showing prominence. The radiometric technique, the focus of this article, measures the naturally occurring radiation present in geological material (Minty, 1997), most usually Potassium (^{40}K), Uranium (^{238}U) and Thorium (^{232}Th). These elements decay directly, or via daughter elements, at discrete energy levels (Minty, 1997), and are recorded as gamma ray counts per second (cps). A 4th Total Count measurement of all radioactive sources is also recorded from the full energy spectrum. Different geological material is made up of different combinations of elements, so level of the initial radioactive source may vary depending on the underlying geology present. Surveys can be conducted by aircraft, allowing for large areas to be consistently surveyed. Traditionally these data were used for bedrock and sediment mapping (Martelet et al., 2006), but several local, regional and review studies have investigated the potential of radiometric data when considering peatland mapping (Ameglio, 2018; Beamish, 2014; Reinhardt and Herrmann, 2019; Siemon et al., 2020).

Radiometric data give a direct measurement of the subsurface. Gamma rays emitted from geological material must pass through any overburden present. This overburden acts as an attenuator (Beamish, 2013). Mineral soils may act as an additional source of radiation due to their parent material (Rawlins et al., 2007). Peat soils, however, have unique attenuation properties due to low bulk density, high porosity and pore saturation, and little radioactive parent material to contribute to the signal. Very low radiometric signal may therefore, be indicative of peatlands within the landscape (Beamish, 2014). Previous studies have chosen the boundary between peat and non-peat soils within radiometric data arbitrarily (Beamish, 2015), based on average observed values of potassium (Berglund and Berglund, 2010) and in combination with other airborne datasets (Siemon et al., 2020). A method of edge detection, Horizontal Gradient Magnitude, used in potential field studies can act to remove this subjectivity (Beamish, 2016). However, the increased use of machine learning for mapping applications may be more suited to an objective identification of peatland extent (Hird et al., 2017; Minasny et al., 2019; Zhang et al., 2017). No radiometric studies on peatland area mapping to date have included machine learning methods, such as those described in this paper.

The aim of this paper is to develop a technique to investigate the potential of airborne radiometric data to complement and improve regional and local scale mapping efforts to delineate the extent of peatlands. To achieve this, modelling the attenuation of three normally recorded elements was performed to highlight potential statistical differences between these data acquired over peat and non-peat soils. Such differences may then be exploited by a supervised machine learning algorithm. An existing national peatland database (Republic of Ireland) was selected to provide training areas for this algorithm. Ireland has between 11,000 km^2 and 16,500 km^2 of peatlands (Connolly and Holden, 2009; Xu et al., 2018), the range highlighting the uncertainty in the various mapping techniques used. Three national databases are available which outline peatland area. These are the CORINE 2018 (CLC18) landcover (CORINE, 2018), the 1:250 k Irish Soil Information System (ISIS) (Creamer, 2014) and the 1:50 k Quaternary Geology Map (QGM) (GSI, 2022a) databases. Their validity is confirmed below using Loss on Ignition (LOI) (Heiri et al., 2001) analysis from a national soil sampling campaign.

An updated peatland area map was then produced using datasets acquired during a national airborne survey called Tellus. These methods may be used to update national and international extent of peatlands, facilitating C emissions estimates, and informing restoration projects.

2. Materials and methods

2.1. Airborne radiometric data

The Tellus survey is an airborne geophysical survey commissioned by the Geological Survey of Ireland (GSI, 2022c). It began in 2012 and to date approximately 80 % of the land area of the country has been covered. The survey acquires coincident Electromagnetic, Radiometric and Magnetic data. The radiometric data are of interest in this study.

The survey is acquired in acquisition "Blocks" which cover large geographic regions. Each block has a similar acquisition geometry; however, some equipment differences exist between acquisition blocks. Survey lines are flown at 345°, with a line spacing of 200 m. Radiometric data are acquired with a 1 Hz frequency, which approximates to a 60 m inline spacing. The nominal survey altitude is 60 m, however occasionally this is exceeded due to terrain or flight restrictions/requirements. Data from all blocks undergo similar processing performed by the contractor (SGL, 2017) in line with international guidelines (IAEA, 2003).

This study uses data from Block A2 of the Tellus airborne survey (Fig. 1). These data were acquired between June and October 2016 and consist of 115 flight lines and 43,141 line kilometres. This block covers most of mid-west of Ireland, approx. 7,900 km^2, and consists of 652,950 individual data locations. These data were acquired in Irish Transverse Mercator (ITM, EPSG 2157) and all datasets used in this study have been re-projected to this reference system. Alongside geographic coordinate, elevation, and altitude specific data, 4 radiometric datasets were used in this study. These are the Potassium (K), Uranium (U), Thorium (Th) and Total Count (TC) data. These data were provided in concentration units, with an approximate depth of investigation of 40–60 cm (Beamish, 2013). In this study, a sensitivity factor (SGL, 2017) for each element was used to transform these data back to counts per second (cps), which is required when considering radiometric attenuation equations (Eqs. (3.1) & (3.2)).

Finally, each data channel was interpolated using minimum curvature to a 50 m × 50 m grid. QGISv3.16 was used for visualisation and GIS analysis (Fig. 1).

2.2. Topsoil survey

The Tellus topsoil survey provides a shallow (0.2 m) and deep (0.5 m) topsoil geochemical analysis, with one survey site per 4 km^2. Since 2011 approximately 50 % of the country has been covered.

Loss on ignition (LOI), used as a measure of the organic content of the sample (Heiri et al., 2001), was extracted from this dataset for both shallow and deep samples within the Tellus airborne A2 block, which contains 1,849 sample locations. A high LOI (>50 %) is indicative of peat soils, or soils with high organic content in Ireland (Creamer and O'Sullivan, 2018). An average LOI was calculated from the shallow and deep samples in order to provide a single representative LOI for a sample location. There are insufficient LOI data to incorporate in the machine learning approach described in Section 2.4.

2.3. National peat databases

The CLC18 landcover classification is the most recent release from the European Environmental Agency (EEA). This is a European landcover classification program, which has produced standardised landcover classifications, derived from satellite remote sensing data products by national teams, at several reference years from 1990 until 2018. The dataset consists of 44 landcover classifications (Kosztra et al., 2017) with peat extent mapped using the classification of "Peat bogs" and "Moors and Heathlands". This database has a minimum mapping unit (MMU) of 25 ha (0.25 km^2), a minimum linear feature resolution of 100 m and a reported thematic accuracy of 85 % (CORINE, 2018).

The QGM is a national map produced by the Geological Survey of Ireland at a 1:50 k (1 cm = 500 m) scale. It aims to map the thickest unit in the top 1 m of the subsurface (GSI, 2022a). This is achieved primarily via traditional mapping techniques, boreholes, and ground geophysical surveys. No overall accuracy is reported for this database, however traditional mapping techniques often have most uncertainty at boundaries of mapped units (Zhang et al., 2017). Ongoing surveys aim to increase overall confidence (GSI, 2022b). This database consists of 83 classifications of sediment types. Peat is classified as "Blanket Peat", "Cut over raised Peat", "Fen Peat" and "Raised Peat (intact)".

The ISIS database is a probabilistic soil association map produced by the Environmental Protection Agency (EPA) and national agriculture

Table 1
Landcover classes removed from Tellus A2 Block Area.

Landcover classes removed:		
Airports	Urban (all)	Intertidal flats
Beaches, Dunes, Sands	Dump/Mineral Extraction sites	Water (Lakes/Rivers)
Coastal Lagoons	Industrial areas	Sea

and food authority (Teagasc) at 1:250 k (1 cm = 2,500 m) scale. It was produced in a machine learning framework using legacy soil maps, environmental co-variates and validation datasets (Creamer, 2015; Creamer and O'Sullivan, 2018). The classification system divides the soils of Ireland into 11 Great Groups following World Reference Base (WRB) principles. Peat is classified under "1xx" relating to the Great Group classification of 1 for peats in Ireland. The accuracy of this database to predict soil types has reported values about 30–40 %.

These databases can be used to remove areas from the study site that are not relevant and to identify training areas for use in the machine learning algorithm (Table 1). All databases were clipped to the Tellus Block A2 boundary. Polygons related to water bodies, urban centres and other non-relevant landcover or subsurface types were merged from all three national databases to produce a maximum extent mask layer of exclusion zones. Radiometric data acquired in these exclusion zones are removed.

Each national database was then simplified into "Peat", based on the relevant database definition, or "non-Peat" areas, by merging the remaining polygons, which provide the training areas. Comparison with LOI definition of peat showed that all three national databases were suitable for use in defining training areas (QGM: 86.4 %, CLC18: 86.2 %, ISIS: 83.1 % agreement), however the QGM was selected as it best matches the expected penetration depth of radiometric data (Beamish, 2013). A more detailed justification for selection of the QGM can be found in Appendix A. Fig. 2 highlights the full workflow.

2.4. Machine learning supervised classification

Classification is the process of grouping together data which share common properties into a set of classes (Delgado et al., 2017). Machine Learning (ML) algorithms are suited to this task, especially where the underlying relationship in the data set is poorly understood (Valentine and Kalnins, 2016) and rely on pattern recognition and statistical relationships as opposed to a pre-determined mathematical model (Dramsch, 2020). In supervised classification, a subset of data is associated with an *a priori* set of "classes". A statistical relationship is found between the input data and the associated class (Dramsch, 2020; Shen, 2018). This relationship can be exploited to predict the classification of new data. Therefore, the input data need to be a good representation of the relationships of interest.

In this study, supervised machine learning classification was used. Machine learning can exploit the statistical differences between the radiometric data layers, where traditional geophysical (i.e., inversion) or numerical (i.e., regression) techniques may not due to the complexity of radiometric data (Reinhardt and Herrmann, 2019). The QGM database provided the *a priori* (target) for supervised classification.

In order to ensure the input data selected to "train" the artificial neural network (ANN) were acquired over the subsurface type of interest, a 200 m buffer zone was defined along either side of all peat boundaries in the QGM and no training data were selected from within the buffer zone. "Peat" classed radiometric data were selected from the remaining peat areas of the QGM outside this buffer zone. This was done to reduce the uncertainty of the QGM areas chosen as training sites, as the most uncertainty in traditional mapping techniques exists at boundaries of mapped unit (Zhang et al., 2017). This also removes any potential overlap between these classes due to the radiometric acquisition footprint, approx. 180 m radius (Minty, 1997). No other filtering of the data was performed.

A total of 168,414 radiometric data points were extracted from within the remaining "peat" area. The same number of datapoints were

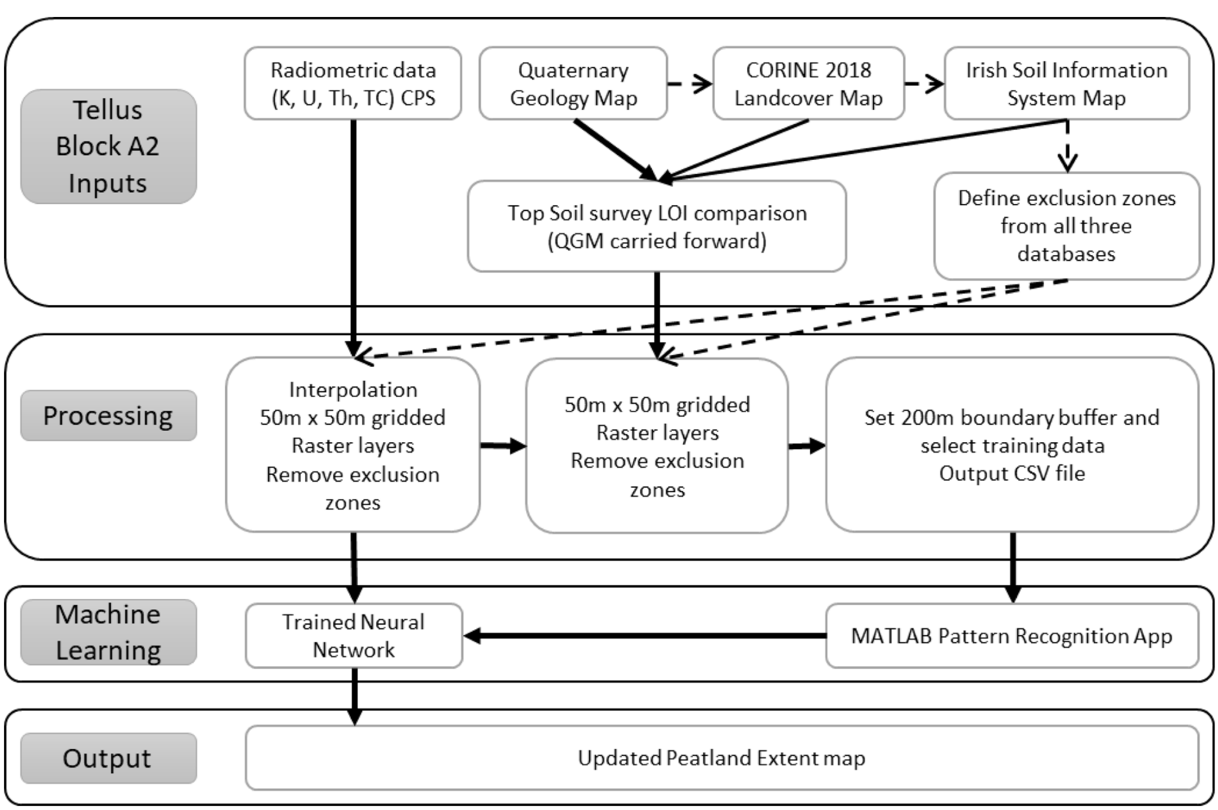

Fig. 2. Workflow Diagram.

extracted randomly from within the "non-peat" areas. These datapoints contain 4 data predictors, K, U, Th, and TCs (cps), and a classification of non-peat (value = 2) or peat (value = 1). Normalisation was applied to bring each radiometric dataset to a common scale (between 0 and 1). These labelled data form the training data within the machine learning framework.

The main assumption in the machine learning training, and subsequent application, is each datapoint is representative of radioactivity from a 50 m × 50 m square produced during interpolation of the airborne radiometric data. The 90 % contribution footprint of radiometric data acquired at 60 m altitude is an approx. 180 m radius circle (Minty, 1997). As the aircraft is moving and recording every 1 *sec*, in reality this area becomes an ellipse. However, the greatest contribution to the signal is from directly below the aircraft and so the interpolation is considered standard in radiometric studies.

This work utilises the MATLAB™ Pattern Recognition Application, which uses a scaled conjugate gradient backpropagation network (Møller, 1993) with the default of 10 hidden layers for machine learning classification sufficient to capture the complexity of the relationships between the input data and the classification. The input data were the normalised four radiometric datasets, which removed any scale differences between the data. The target classes were defined as "non-Peat" or "Peat". The input dataset was randomly divided into training (70 %), validation (15 %) and testing (15 %), a standard procedure when training an artificial neural network (ANN). A confusion matrix (Ting, 2010) for all the input data is then used to access the success of machine learning training.

2.5. Theory/Calculations

Radiometric data are often presented as a map, which is representative of each element's concentration within an approximate depth of the subsurface, similar to Fig. 1. This depth has previously been explored via modelling of gamma ray attenuation in subsurface materials (Beamish, 2013) and quantification of a depth of penetration for various overburden types, with "wet peat" being 60 cm and mineral soils between 40 and 60 cm. This represents the depth in each material within which 90 % of the radiometric signal is originating.

The general assumption is that bedrock is the radioactive parent material present in mineral soils (Beamish, 2015; Priori et al., 2014; Rawlins et al., 2007), which contributes to the radiometric signal acquired at the aircraft. However, peats are considered to be a non-radioactive overburden, with the exception of reported uranium enrichment (Vodyanitskii et al., 2019) in certain cases.

2.6. Radiometric attenuation

The measured gamma ray flux (I_m) can be considered as a gamma source with an intensity (I_o), measured in photon rate per second of emission, which has been reduced after passing through some material. In crustal materials (rocks), gamma ray sources are radionuclides present since the formation of the planet and are dependent on the material's geochemistry (Minty, 1997). Attenuation of this gamma emission is exponential and related to a linear attenuation coefficient (μ) of the material through which the gamma ray passes, and the thickness (x) of the material (Davisson and Evans, 1952).

The linear attenuation coefficient can be described as the mass attenuation coefficient (μ_m) multiplied by the density (ρ) of the material. The mass attenuation coefficient is related to the number of electrons present in a material. The full equation for gamma ray flux measurement is given by the following:

$$I_m = I_o exp(-(\mu_m \times \rho)x) \tag{3.1}$$

A more appropriate equation was proposed (Endrestøl, 1980) and further explored by (Beamish, 2013) which resulted in a three-phase system which accounts for the three phases of geological material, solid (s), water (w) and air (a). An additional step is added here to account for the passage of the gamma rays through the air to the detector at aircraft altitude. This results in a 4-phase system of one-dimensional (1D) attenuation from an underlying source to a detector at aircraft altitudes (Equation (3.2)).

$$I_m = I_O exp\left(-\left(\begin{array}{c}[(\mu_s \times \rho_s) \times (1-\varnothing) \times x] + [(\mu_w \times \rho_w) \times (S\varnothing) \times x] \\ +[(\mu_a \times \rho_a) \times (\varnothing(1-S)) \times x] + [\mu_{al} \times h]\end{array}\right)\right. \tag{3.2}$$

where

$\varnothing$ = Porosity (Volume of void spaces) expressed as a decimal percentage.

S = Saturation (Volume of liquid within void spaces) expressed as a decimal percentage.

$\mu_{s/w/a}$ = Mass attenuation coefficient of solid/water/air (Minty, 1997) for an energy range.

$\rho_{s/w/a}$ = Bulk density of solid (variable), water (1) or air (0.001293) expressed in g/cm^3.

x = thickness of layer expressed in cm.

μ_{al} = Linear attenuation coefficient of air per metre (as provided by the survey contractor, (SGL, 2017)).

h = production altitude (60 m).

For each aircraft observation point, there are 3 independent data (K, U and Th) and 5 unknown parameters (equation (3.2)), so it is an underdetermined system of equations. This means that the same data can be modelled with many combinations of the parameters of the non-radioactive medium. It is not possible to estimate, e.g., the thickness of peat, without additional ground-based constraints on the other parameters, especially for areas where peat thickness > 60 cm will substantially reduce the signal to noise ratio.

This equation (equation (3.2)) can be used to produce a simple 1D model of gamma ray attenuation of some initial source intensity (cps) passing through a non-radioactive medium, with the attenuation being controlled by the physical properties of that medium. These are media density (g/cm^3), porosity (%), saturation (%), and layer thickness (cm). All three recorded elements (K, U and Th) can be modelled using specific attenuation coefficients for each (Minty, 1997). TC data cannot be modelled as they represent an integration of the full energy spectrum detected and no one attenuation coefficient can be used.

Table 2
Physical Properties used in modelling radiometric attenuation. Initial intensity refers to the counts per second intensity directly underlying the attenuating material. Bulk Density refers to the material density of the overburden. Porosity refers to the volume of void spaces. Saturation refers to the filled void spaces. Thickness refers to the constant vertical thickness of the overburden.

Physical Property	Peat	Non-Peat
Initial Intensity (cps)	K, U, Th = 500 ± 50 cps	
Bulk Density (g/cm^3)	0.01 – 0.25	1.1–1.65
Porosity (%)	90 – 99	30 – 70
Saturation (%)	80 – 100	10 – 70
Thickness (cm)	50	50

2.7. Modelling peat vs non-peat attenuation effect

Modelling was performed using equation (3.2) to produce a theoretical radiometric dataset of K, U and Th responses from one million models of random combinations of typical subsurface physical properties for peat and non-peat in Ireland (Table 2) (Galvin, 1976; Kiely and Carton, 2010).

The initial intensities were allowed to vary randomly within defined limits (Table 2) to replicate the probabilistic nature of radioactive decay in a given time window (Minty, 1997). Thickness has the most influence on radiometric attenuation (Beamish, 2013), but is not an intrinsic

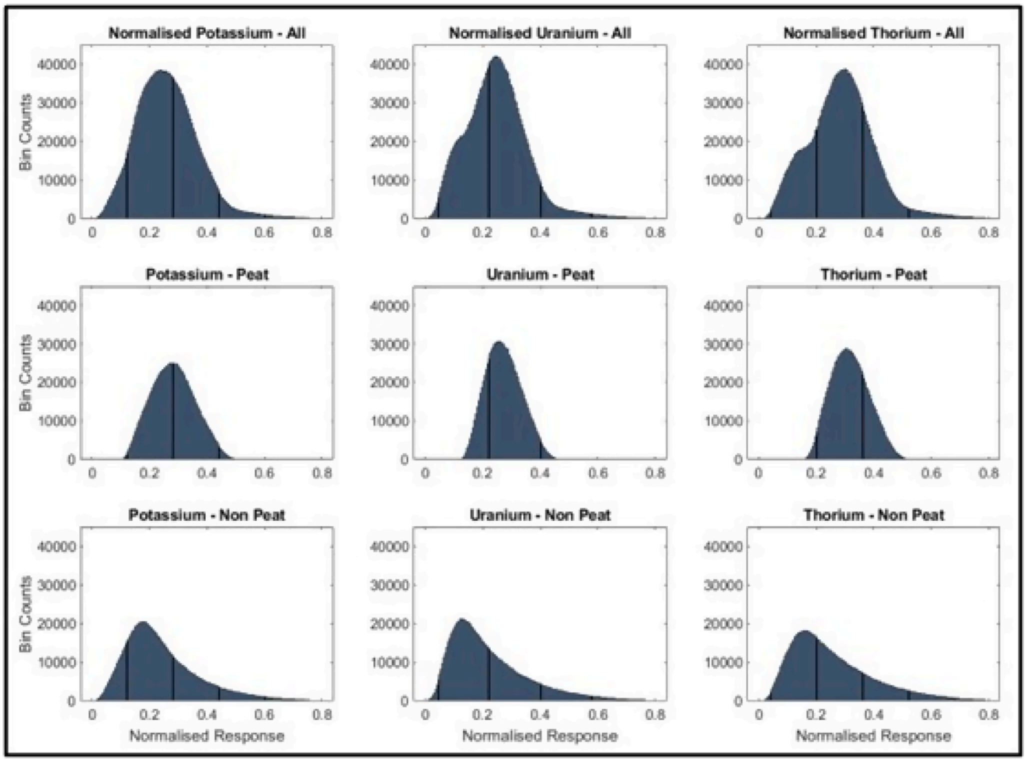

Fig. 3. Histogram analysis of modelled radiometric data, showing distribution and response difference for each radiometric element and modelling scenario.

physical property of the overburden. In order to observe radiometric attenuation due only to property differences, the thickness remained constant (50 cm) for all models. Each model is a 1D representation of vertical gamma ray attenuation of 3 elements (K, U, Th) from source to aircraft, passing through a three-phase overburden of constant thickness, variable physical property values, and a 60 m air column.

The final element in modelling radiometric data is the addition of random noise. This represents noise in real radiometric data that is not corrected during processing, such as small aircraft motion. Noise estimates were taken from Tellus Block A2 data. Noise calculated using Beamish (2013)) resulted in levels of $K_n = \pm 6.76$ cps, $U_n = \pm 2.42$ cps, $Th_n = \pm 2.32$ cps. Noise was independently and randomly assigned within these limits to each model dataset.

This yields two million datapoints with a modelled K, U, Th response and classification of peat or non-peat. All responses were normalised to fall between a minimum of 0 and a maximum of 1, a standard part of any machine learning workflow (Valentine and Kalnins, 2016). A histogram analysis is used to visualise the responses for each element/modelled overburden combination and a correlation analysis is used to examine the relationships between the responses within each modelling scenario.

3. Results and discussion

3.1. Modelling radiometric attenuation in peats and non-peats

The purpose of the modelling exercise was to conceptualise the statistical differences, existing between radiometric responses acquired over non-radioactive peat compared to those acquired over non-peat overburden, which would be exploited by an ANN. A histogram was used to display the two million modelled responses (Fig. 3), where rows show modelling scenarios and columns show the three different element responses. The top row shows the response from all 2 million models. The middle row shows the 1 million responses when modelled using peat physical properties and the bottom row shows the responses when modelled using non-peat physical properties.

The top row highlights an important observation. The U and Th responses exhibit a slight bi-modal distribution, when compared to K responses. The middle and bottom rows reveal that the peaks in the top row line up with the peat modelled responses, indicating that the attenuation responses in a peat, compared to a non-peat model, are becoming notably different at higher gamma ray energies. Th responses from peat models are less attenuated compared to K responses, whereas non-peat models display similar attenuation across all three elements (Fig. 3).

The reason for this can be determined from Equation (3.2) and the range of physical parameters used to define a peat and a non-peat (Table 2). The very low bulk density (<0.25 g/cm^3) and very high saturation and porosity values attributed to peat (Galvin, 1976) mean that the attenuation of gamma rays in peat models is controlled mostly by the given porosity and saturation. This coupled with a stronger attenuation coefficient for K compared to U and Th means that as gamma energy increases, attenuation decreases for peat models.

Non-peat models, by comparison, have a larger bulk density (1.1 – 1.65 g/cm^3) and a larger potential range for porosity and saturation (Table 2) (Kiely and Carton, 2010). Therefore, the attenuation of a non-peat model is controlled by the combination of physical parameters, including a more significant impact from the bulk density of the solid component of the model. This results in more consistent attenuation regardless of gamma ray energy.

An interesting observation of this analysis is that, given a non-

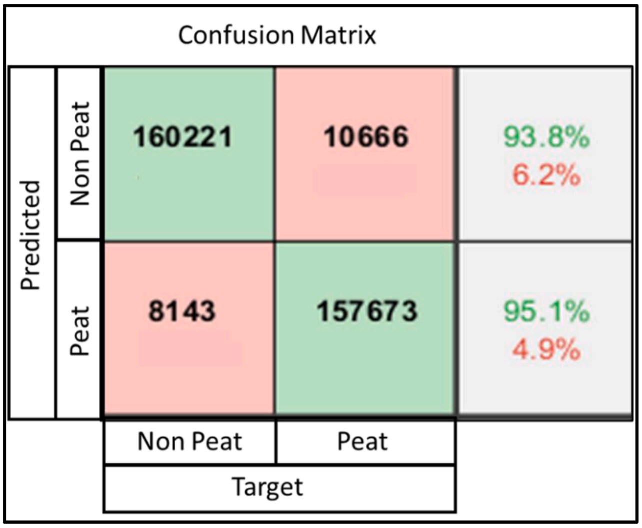

Fig. 4. Confusion matrix showing the training success. Coloured squares show number of data points either re-classified or un-changed. Grey squares represent percentage of matching classification i.e., 95.1% of the data predicted to be "peat" was originally classified "peat" in the QGM and remain un-changed. 4.9% have been re-classified as "peat" by the neural network from "non-peat" in the QGM.

radioactive overburden and a constant depth, non-peat models have an increased and more consistent attenuation across the three elements when compared to peat models. This appears to be counter-intuitive to published literature which highlight peatlands as strong attenuation areas within radiometric surveys (Beamish, 2014; Siemon et al., 2020). However, the models presented here do not consider the effect of parent material in non-peat soils, which will effectively mask any underlying radiometric source signal (Rawlins et al., 2007; Reinhardt and Herrmann, 2019). The lack of parent materials in peats result in areas of low radiometric signal in radiometric surveys in addition to the attenuation strength of a peat soil. This observation highlights another "radiometric difference" between peat and non-peat soils, in that peat soils act as an attenuating medium, whereas non-peat soils act as both a source and attenuator of radiometric signal.

The distributions of each of the histograms are determined by the range of physical parameters used in each model (Table 2). As this range is unknown for any real-world survey, recorded distributions may not match this modelled scenario. However, the differences *between* the data may be of use. In order to show this, a correlation analysis was performed separately for peat and non-peat modelled datasets to show how one modelled dataset changes with respect to another within each modelling scenario.

Radiometric responses modelled with peat physical properties are less correlated compared to responses modelled using non-peat properties. The combination of two things results in this lower correlation: (1) the sensitivity of the radiometric responses in peat to the relevant attenuation coefficients and (2) the introduction of randomness in the form of initial intensity and noise, which naturally decreases correlation between datasets. Here, however, the randomness is applied equally to both peat and non-peat modelled radiometric responses. The greater sensitivity to attenuation coefficients in peat modelled responses results in the random noise having an increased effect compared to non-peat modelled responses.

It is noted that the level and randomness of the initial source intensity are estimates, and there is no empirical evidence for their choices, however normalisation removes the importance of their relative strengths. The noise levels used are orders of magnitude lower than the chosen initial signal. Decreasing the initial signal level decreases the correlation and the removal of randomness results in near perfect correlation in both modelling scenarios.

3.2. Machine learning training

A confusion matrix is used to describe training success (Fig. 4). This matrix shows how successful the ANN is at classifying the training data (described in 2.4) using the labels provided (Ting, 2010). The "target" is the classification pre-assigned to each data point, the "predicted" refers to the classification assigned by the ANN post training.

The overall training success indicated that 94.4 % of all training data were classified the same as the QGM (with the buffer zone) by the neural network with 5.6 % being re-classified by the neural network. It is likely that some mis-classified QGM areas were still present, despite the caution of the 200 m buffer zone, as shown by this re-classification. An analysis with a buffer zone of 300 m either side of the QGM boundaries resulted in a marginal improvement in the classification accuracy to ~96 %. ANN has therefore identified a statistical model to differentiate between radiometric data acquired over peat and non-peat overburden and can now be applied to the full Tellus A2 block dataset.

3.3. Updating the peatland map

All datapoints from the Tellus Airborne A2 block were normalised with the same parameters as the training data and passed to the trained ANN, which outputs a classification of peat or non-peat (Fig. 5-A).

This updated peatland map can be compared to the QGM database (Fig. 5-B). Both peatland extent maps show good agreement, as expected as the ANN was trained using the QGM. By calculating a difference (Fig. 5-E), areas that were reclassified by the ANN can be seen. This difference map shows that the results are not significantly influenced by the underlying geology (Fig. 5-C) or topography related high fly zones (Fig. 5-D), both important considerations in radiometric studies (Beamish, 2015; Minty, 1997).

Underlying geology may influence the initial source intensity as well as contribute to the parent material of the soil, both having an effect on the recorded radiometric signal (Beamish, 2015; Rawlins et al., 2007). Complex topography can decrease the quality of radiometric data due to rapid changes in aircraft altitude to maintain terrain clearance (Fig. 5-D). There may also be non-vertical gamma rays originating from valley sides (Minty, 1997; Reinhardt and Herrmann, 2019).

The ANN classification result contains interesting features when compared to the other databases. The resolution of the three national databases is controlled by mapping units and accuracy measurements. The ANN result is based on individual 50 m × 50 m squares, which represent the resolution of this database. However, any isolated classified square is therefore more likely to be a product of noise than a correct classification and may require the use of a spatial filter. However coherent groups of similar classification are likely to be true classifications. The argument for increased resolution is furthered by the fact that each 50 m × 50 m area has been derived from a *direct measurement* of the subsurface. This is compared to a surface (1 cm – 2 cm depth) measurement present in the CLC18 database, and only sparse subsurface measurements present in QGM and ISIS databases. These traditionally derived maps resolutions may also be affected by local issues, such as access to land to validate soil type, which will not affect the results of an

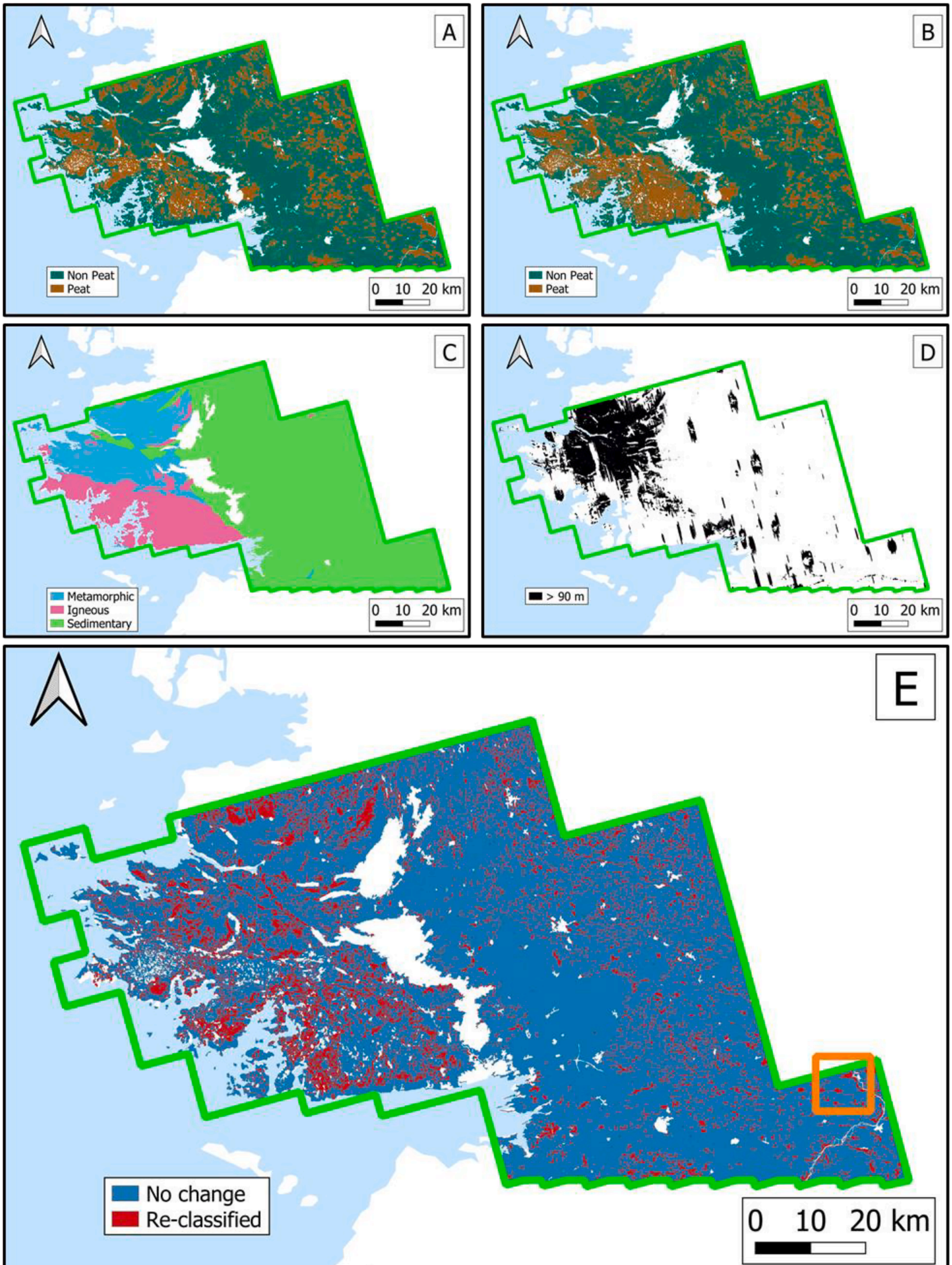

Fig. 5. Radiometric based peat map. A) ANN Classified peatland area. B) QGM database peatland area. C) Simplified Geology map. D) Tellus Survey > 90 m clearance from ground E) Red = areas that the ANN is different to the QGM. Blue = the classification is the same as the QGM. Orange boundary is study site detailed in Section 4.3.1. A, B, D and E Maps have exclusion zones removed.

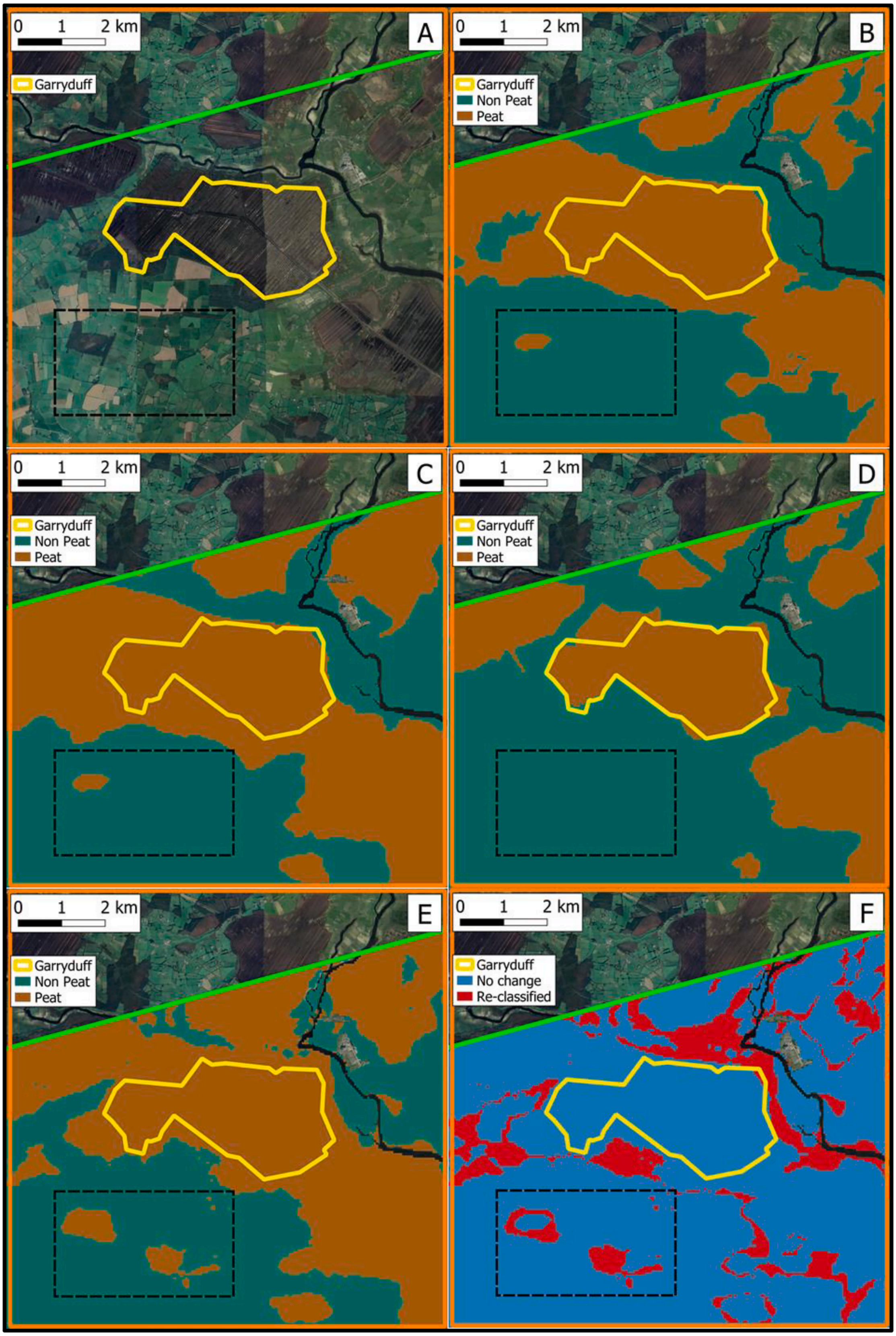

Fig. 6. A) Google image of study area. Yellow boundary defined from commercial surveys on site. Black Dashed area highlighting two sites identified as peat by ANN classification, seen as dark green (forest) and light green (grass). B) Simplified QGM database of study area. C) Simplified ISIS database of study area. D) Simplified CLC18 database of study area. E) ANN classification of study area. F) Difference between B and E.

airborne survey presented here.

While the effect of geology is partially accounted for via regional spatial sampling within machine learning training, the decrease in spatial resolution of radiometric data due to complex topography and high fly zones is unavoidable, as the area from which gamma rays originate expands greatly with increased clearance above the surface (Reinhardt and Herrmann, 2019). Although a linear correction is applied to correct the data to production altitude (SGL, 2017), the effect of complex topography cannot be accounted for. Therefore, while there is still a valid statistical relationship present in the recorded radiometric data in mountainous regions, the area from which the gamma rays originate is not well constrained. Therefore, any result from mountainous regions, such as the western portion of the study area (Fig. 5-E) would require extensive ground truthing and combination with other peatland area datasets (Connolly et al., 2007) to assess accuracy.

3.4. Predicting peatland extent in flat terrain

In contrast to mountainous regions, relatively flat terrain exhibits no such complexity. The remaining discussion will highlight an example of the proposed method's ability to update the extents and spatial distribution of peatlands centred on a former industrial extraction site.

The chosen site is located at the eastern side of the Tellus A2 block (Fig. 5-E). It is known locally as Garryduff bog and until recently was harvested for material to generate electricity at a nearby power plant. This site was chosen for this study as it provides a representation of a typical industrial peatland site in the northern hemisphere and surrounded by grassland and some forestry.

All three simplified national peatland databases are shown (Fig. 6-B/C/D) highlighting the differences in peatland extent and spatial distribution. Each database can be visually compared to the aerial image, which outlines the Garryduff bog (Fig. 6-A). The QGM and ISIS databases show peat extent outside the Garryduff boundary and show a connection between other peatland areas. The CLC18 shows increase in peatland extent.

The direct measurement has another implication for the ANN classification, namely that it may "see through" landcover. In particular, the radiometric data may detect peatlands under anthropogenically modified land use, such as grass or forest. This is evident in the study area (Fig. 6-E) as the ANN classification has detected two distinct areas of peatland in the south-western quadrant of the study area (black dashed box). These are partially detected on the QGM and ISIS databases, and not detected on the CLC18 database. The CLC18 database identified these areas as "Mixed Forest" and "Pasture" (west to east). The QGM identifies these areas as "cut over raised peat" and "Till derived from limestone" respectively. The ISIS identifies these as "peat" and "fine-coarse loamy drifts with limestone". The ANN classification shows that these areas are larger than previously identified. It is noted that these areas were not included in training data (Section 4.2) for the ANN due to the buffer zone, but are still identified as peat by the ANN. See Appendix B for zoomed images for each of these sites.

This result is also relevant for currently known peatlands, such as the Garryduff site. The ANN classification has extended the boundaries beyond this industrial peatland (red boundary) into the surrounding areas. The difference (Fig. 6-F) shows areas of the site that have been reclassified by the ANN classification, compared to the QGM, which highlights the increases in resolution provided by this method.

The radiometric signal has been shown to be affected by vegetation cover (Reinhardt and Herrmann, 2019), which can act as both an attenuator or a source of radiation. Within this study site, ANN classified areas are not strictly following visible vegetation boundaries (Fig. 6-E), such as forests. This leads to the conclusion that the presence of vegetation (e.g., grass and forest) may not affect the classification of the underlying subsurface. As results from radiometric attenuation modelling have shown, peat has a distinctive attenuation signature in radiometric acquired data when considering all recorded radiometric datasets, which may be independent of vegetation cover.

4. Conclusions

The methods presented can be used for international peatland mapping projects where similar datasets exist and may provide important updates to peatland inventories by identifying areas of previous unrecognised peat and updating boundary locations for established peatland sites. This has implications for global carbon stock assessment, rehabilitation projects and land management decisions. The method is reliant on good quality airborne radiometric data and some *a priori* knowledge of peatland extent in order to provide appropriate training areas. These areas should be spatially distributed across the full study site in order to capture any effects of changing geology to the radiometric data. As the method relies on statistical relationships between all recorded radiometric datasets, it is more suited to large areas and large datasets. Smaller areas may not exhibit such statistical relationships as clearly, as the range of attenuation properties may be limited. Once a large area has been classified, however, the results can be used as a product for more focused localised studies or incorporated into other peatland mapping projects.

Declaration of Competing Interest

The authors declare that they have no known competing financial interests or personal relationships that could have appeared to influence the work reported in this paper.

Acknowledgements

The research conducted in this publication was funded by the Irish Research Council under grant number GOIPG-2018-233. Contains Irish Public Sector Data (Geological Survey Ireland) licensed under a Creative Commons Attribution 4.0 International (CC BY 4.0) licence. The authors wish to acknowledge Prof. Mark Healy (NUIG), Prof. Owen Fenton (NUIG/Teagasc) and Dr Pat Tuohy (Teagasc) for their constructive comments during the production of this paper. Many thanks to the two anonymous reviewers for providing insightful feedback leading to a much improved article.

Appendix A

Quaternary Geology Map for ANN training

The correct selection of training areas, where the presence of peatlands is well known, is vital for a machine learning methodology to be successful. Given three national databases which describe peatland in the study area, the challenge is to select one to use for training of the neural network. As noted, (section 2.3), all three databases matched with LOI analysis. The application of a 200 m buffer zone is also considered necessary to account for the airborne radiometric footprint to reduce misclassification (section 2.4). The final analysis was to determine which database, after the application of a 200 m buffer (Fig A.1), had the most overlap with the other databases (Table A.1).

The QGM (with buffer zone) was chosen as it firstly matched with LOI data. Secondly it had the largest overlap with the other peatland extent databases available (Table A.1) meaning that it was limited to areas where all three databases reported peat to be present. Finally, it was also the most conservative in terms of peatland extent (Fig A.1-B), which would focus training to localised areas where peat was likely to be present.

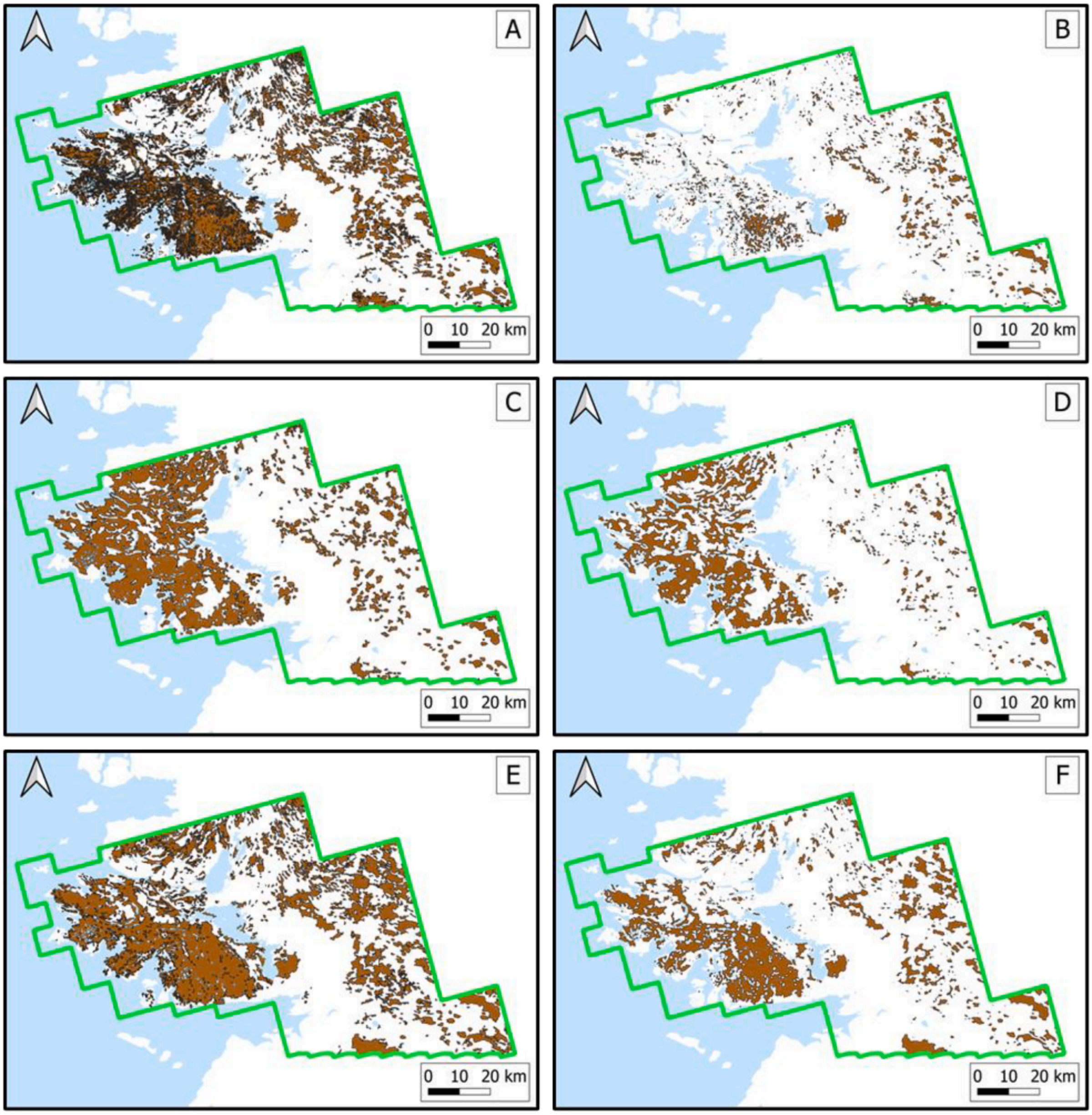

Fig A.1. Existing peatland extent maps within Tellus Block A2 A) QGM, B) QGM with 200 m buffer, C) CLC18, D) CLC18 with 200 m buffer, E) ISIS, F) ISIS with 200 m buffer.

Table A.1
Percentage overlap between databases with 200 m buffer and each database without a buffer.

	Full QGM % Overlap	Full CLC18 % Overlap	Full ISIS % Overlap
QGM (200 m buffer)	100	70.2	99.4
CLC18 (200 m buffer)	64.7	100	76.0
ISIS (200 m buffer)	83.1	67.2	100

Appendix B

Validation of ANN classification.

Validation of local re-classification was performed via aerial imagery within the Garryduff study site with Aerial imagery were taken from Bing Imagery (https://www.bing.com/maps/aerial). Aerial images were used to verify if two highlighted local sites (Fig. 6) were correctly re-classified as peat, including an updated boundary classification (Fig B.1) and identification of a new peatland site (Fig B.2). Peat was identified on aerial imagery from bare exposure, colour changes and differences to surrounding areas, similar to the main Garryduff peatland.

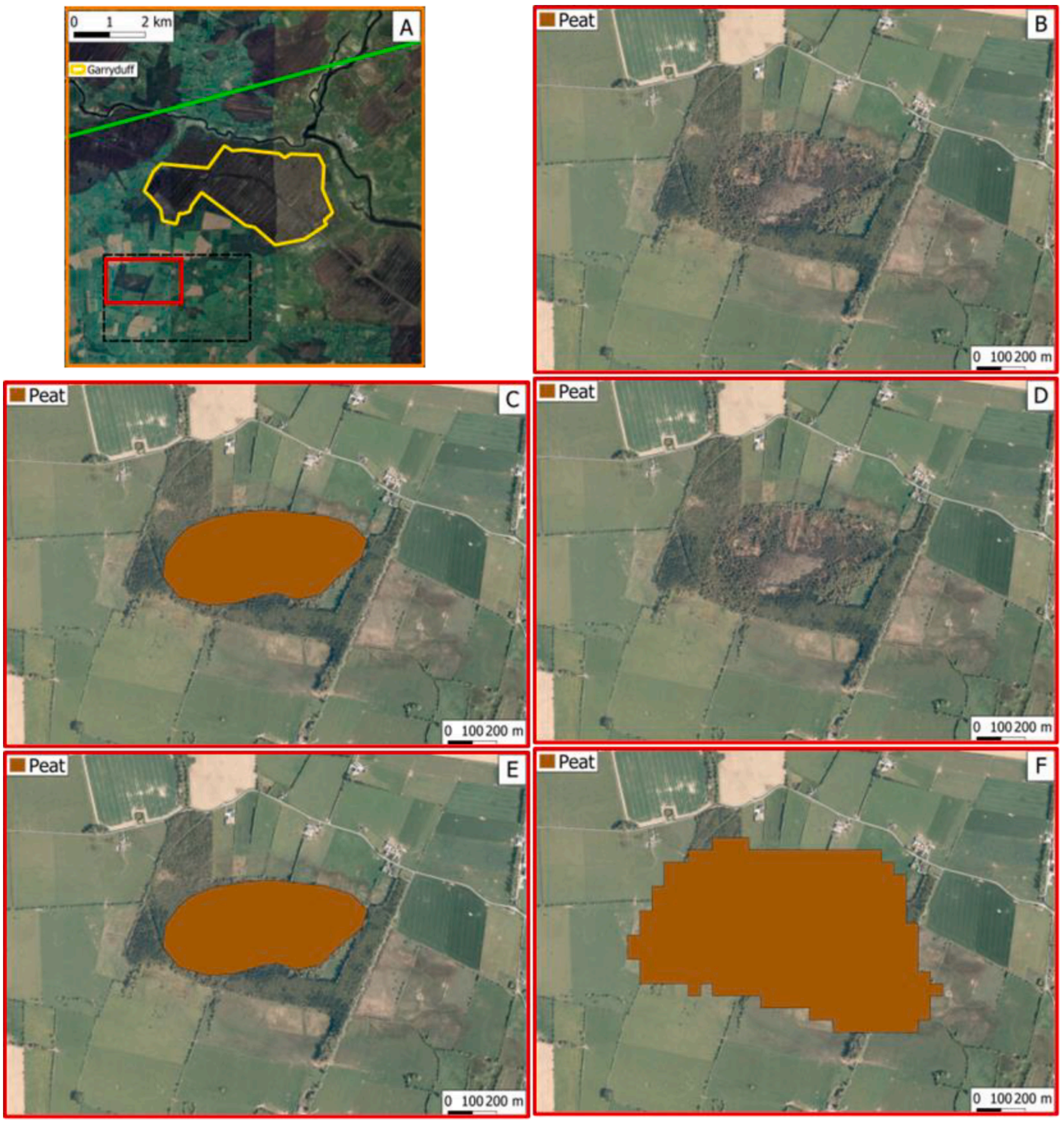

Fig B.1. A) Google image of study area. Yellow boundary defined from commercial surveys on site. Black Dashed area highlighting two sites identified as peat by ANN classification. Red Box shows zoomed area in B, C, D and E. B) Aerial image of zoomed area. C) QGM definition of peat in zoomed area, surrounded by "Till derived from limestone". D) CLC18 definition of peat in zoomed area. CLC18 misclassifies this area as "Mixed forest" surrounded by "pasture" and "Non-irrigated arable land". E) ISIS definition of peat in zoomed area. F) ANN classification of peat in zoomed area.

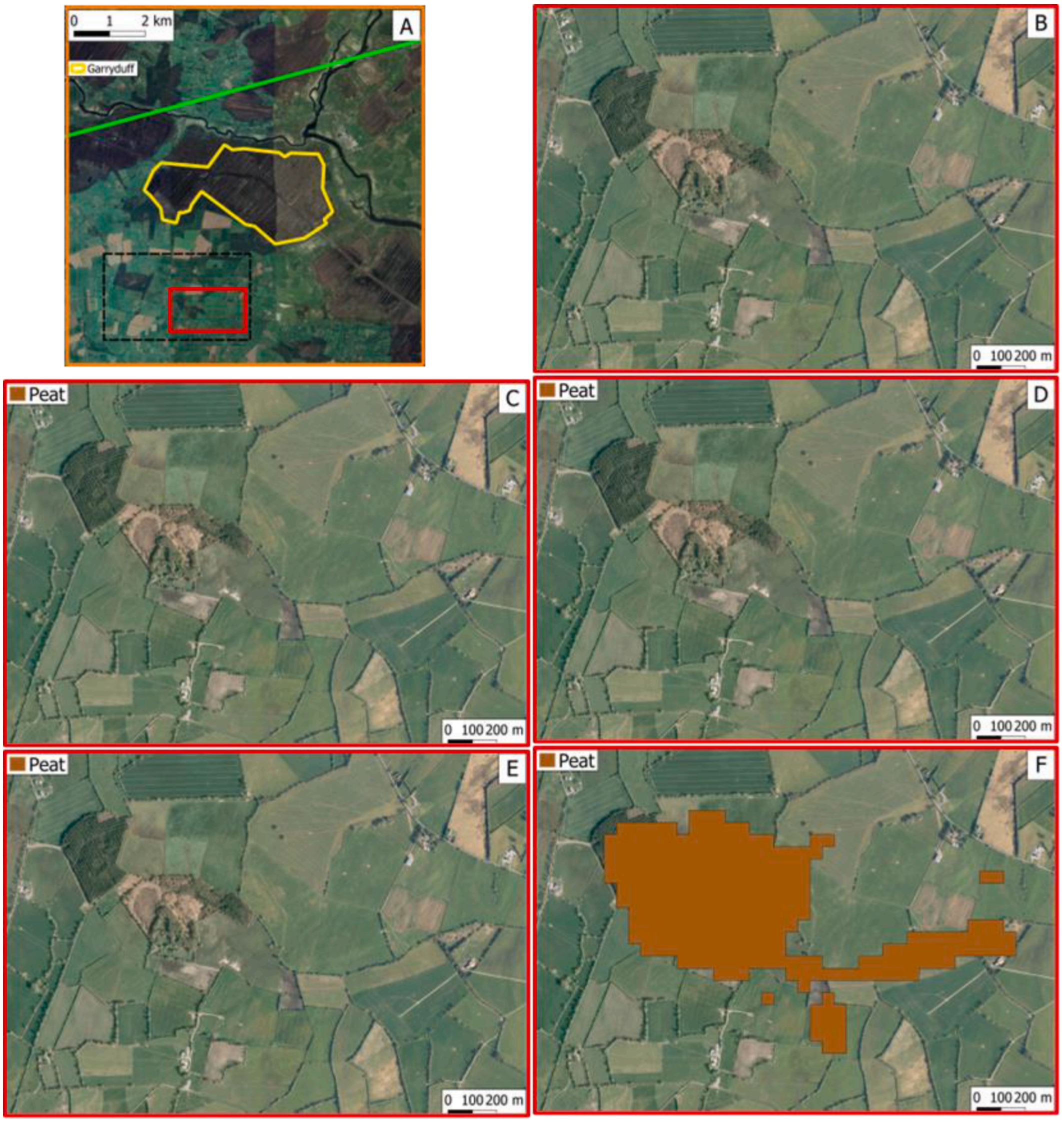

Fig B.2. A) Google image of study area. Yellow boundary defined from commercial surveys on site. Black Dashed area highlighting two sites identified as peat by ANN classification. Red Box shows zoomed area in B, C, D and E. B) Aerial image of zoomed area. C) QGM does not define any peat in zoomed area, classed as "Till derived from limestone". D CLC18 does not define any peat in zoomed area, classed as "pasture". E) ISIS does not define any peat in zoomed area, classed as non-peat soils. F) ANN definition of peat in zoomed area.

References

Airo, M.-L., Hyvönen, E., Lerssi, J., Leväniemi, H., Ruotsalainen, A., 2014. Tips and tools for the application of GTK's airborne geophysical data, Geological Survey of Finland, https://tupa.gtk.fi/julkaisu/tutkimusraportti/tr_215.pdf, (accessed 09/05/2022).

Aitkenhead, M.J., 2017. Mapping peat in Scotland with remote sensing and site characteristics. Eur. J. Soil Sci. 68 (1), 28–38. https://doi.org/10.1111/ejss.12393.

Ameglio, L., 2018. Review of developments in airborne geophysics and geomatics to map variability of soil properties. 14th International Conference on Precision Agriculture. https://www.ispag.org/proceedings/?action=download&item=5024 (accessed 14/04/2022).

Aune-Lundberg, L., Strand, G.-H., 2021. The content and accuracy of the CORINE Land Cover dataset for Norway. Int. J. Appl. Earth Obs. Geoinf. 96, 102266. https://doi.org/10.1016/j.jag.2020.102266.

Beamish, D., 2013. Gamma ray attenuation in the soils of Northern Ireland, with special reference to peat. J. Environ. Radioactiv. 115, 13–27. https://doi.org/10.1016/j.jenvrad.2012.05.031.

Beamish, D., 2014. Peat Mapping Associations of Airborne Radiometric Survey Data. Remote Sens-Basel 6 (1), 521–539. https://doi.org/10.3390/rs6010521.

Beamish, D., 2016. Enhancing the resolution of airborne gamma-ray data using horizontal gradients. J. Appl. Geophys. 132, 75–86. https://doi.org/10.1016/j.jappgeo.2016.07.006.

Beamish, D., 2015. Relationships between gamma-ray attenuation and soils in SW England. Geoderma 259, 174-186. https://doi.org/10.1016/j.geoderma.2015.05.018.

Berglund, O., Berglund, K., 2010. Distribution and cultivation intensity of agricultural peat and gyttja soils in Sweden and estimation of greenhouse gas emissions from cultivated peat soils. Geoderma 154 (3–4), 173–180. https://doi.org/10.1016/j.geoderma.2008.11.035.

Boaga, J., Viezzoli, A., Cassiani, G., Deidda, G.P., Tosi, L., Silvestri, S., 2020. Resolving the thickness of peat deposits with contact-less electromagnetic methods: A case study in the Venice coastland. Sci. Total Environ. 737, 139361. https://doi.org/10.1016/j.scitotenv.2020.139361.

Connolly, J., Holden, N.M., 2009. Mapping peat soils in Ireland: updating the derived Irish peat map. Irish Geography 42 (3), 343–352. https://doi.org/10.1080/00750770903407989.

Connolly, J., Holden, N.M., Ward, S.M., 2007. Mapping Peatlands in Ireland using a Rule-Based Methodology and Digital Data. Soil Sci. Soc. Am. J. 71 (2), 492–499. https://doi.org/10.2136/sssaj2006.0033.

Corine, 2018. European Union, Copernicus Land Monitoring Service 2018. accessed 02/03/2022. https://land.copernicus.eu/.

Creamer, R., 2014. Irish SIS Final Technical Report 8: Correlation of the Irish Soil Classification System to World Reference Base 2006 system. Environmental Protection Agency Ireland, Secure Archive For Environmental Research Data. https://eparesearch.epa.ie/safer/iso19115/displayISO19115.jsp?isoID=3071, (accessed 09/05/2022).

Creamer, R., 2015. Irish SIS Final Technical Report 11: Methodology for the Validation of predictive mapping. Environmental Protection Agency Ireland, Secure Archive For Environmental Research Data. https://eparesearch.epa.ie/safer/iso19115/displayISO19115.jsp?isoID=3064, (accessed 09/05/2022).

Creamer, R., O'Sullivan, L., 2018. The Soils of Ireland. Springer International Publishing, Cham, Cham. https://doi.org/10.1007/978-3-319-71189-8.
Dargie, G.C., Lewis, S.L., Lawson, I.T., Mitchard, E.T.A., Page, S.E., Bocko, Y.E., Ifo, S.A., 2017. Age, extent and carbon storage of the central Congo Basin peatland complex. Nature 542 (7639), 86-+. https://doi.org/10.1038/nature21048.
Davisson, C.M., Evans, R.D., 1952. Gamma-ray absorption coefficients. Rev. Mod. Phys. 24 (2), 79–107. https://doi.org/10.1103/RevModPhys.24.79.
Delgado, S., Higuera, C., Calle-Espinosa, J., Morán, F., Montero, F., 2017. A SOM prototype-based cluster analysis methodology. Expert Syst. Appl. 88, 14–28. https://doi.org/10.1016/j.eswa.2017.06.022.
Donlan, J., O'Dwyer, J., Byrne, K.A., 2016. Area estimations of cultivated organic soils in Ireland: reducing GHG reporting uncertainties. Mires Peat 18. https://doi.org/10.19189/MaP.2016.OMB.230.
Dramsch, J.S., 2020. 70 years of machine learning in geoscience in review. Adv. Geophys. 61 https://doi.org/10.1016/bs.agph.2020.08.002.
Endrestøl, G.O., 1980. Principle and method for measurement of snow water equivalent by detection of natural gamma radiation / Principe et méthode pour la mesure de l'hauteur d'eau équivalente par détection du rayonnement gamma naturel. Hydrol. Sci. Bull. 25 (1), 77–83. https://doi.org/10.1080/02626668009491906.
EU, 2020. 2030 climate & energy framework. https://ec.europa.eu/clima/eu-action/climate-strategies-targets/2030-climate-energy-framework_en#ecl-inpage-910, (accessed 09/05/2022).
Evans, C.D., Peacock, M., Baird, A.J., Artz, R.R.E., Burden, A., Callaghan, N., Chapman, P.J., Cooper, H.M., Coyle, M., Craig, E., Cumming, A., Dixon, S., Gauci, V., Grayson, R.P., Helfter, C., Heppell, C.M., Holden, J., Jones, D.L., Kaduk, J., Levy, P., Matthews, R., McNamara, N.P., Misselbrook, T., Oakley, S., Page, S.E., Rayment, M., Ridley, L.M., Stanley, K.M., Williamson, J.L., Worrall, F., Morrison, R., 2021. Overriding water table control on managed peatland greenhouse gas emissions. Nature 593 (7860), 548–552. https://doi.org/10.1038/s41586-021-03523-1.
Galvin, L.F., 1976. Physical-Properties of Irish Peats. Irish J Agr Res 15(2), 207-&, http://www.jstor.org/stable/25555820. (accessed 09/05/2022).
Gatis, N., Luscombe, D.J., Carless, D., Parry, L.E., Fyfe, R.M., Harrod, T.R., Brazier, R.E., Anderson, K., 2019. Mapping upland peat depth using airborne radiometric and lidar survey data. Geoderma 335, 78–87. https://doi.org/10.1016/j.geoderma.2018.07.041.
GPI, 2016. Global Peatlands Initiative. https://www.globalpeatlands.org/, (accessed 05/04/2022).
Grand-Clement, E., Anderson, K., Smith, D., Luscombe, D., Gatis, N., Ross, M., Brazier, R. E., Wan, S., 2013. Evaluating ecosystem goods and services after restoration of marginal upland peatlands in South-West England. J. Appl. Ecol. 50 (2), 324–334. https://doi.org/10.1111/1365-2664.12039.
GSI, 2022A. National Quaternary Sedement Map 1:50K. accessed 02/05/2022. https://www.gsi.ie/en-ie/data-and-maps/Pages/Quaternary.aspx#Sed.
GSI, 2022b. Quaternary Field Mapping. accessed 02/05/2022. https://www.gsi.ie/en-ie/programmes-and-projects/geological-mapping/activities/Pages/Quaternary-Field-Mapping.aspx.
GSI, 2022c. Tellus Survey. accessed 01/05/2022. https://www.gsi.ie/en-ie/programmes-and-projects/tellus/Pages/default.aspx.
Heiri, O., Lotter, A.F., Lemcke, G., 2001. Loss on ignition as a method for estimating organic and carbonate content in sediments: reproducibility and comparability of results. J. Paleolimnol. 25 (1), 101–110. https://doi.org/10.1023/A:1008119611481.
Hird, J.N., DeLancey, E.R., McDermid, G.J., Kariyeva, J., 2017. Google Earth Engine, Open-Access Satellite Data, and Machine Learning in Support of Large-Area Probabilistic Wetland Mapping. Remote Sens-Basel 9 (12). https://doi.org/10.3390/rs9121315.
Iaea, 2003. Guidelines for Radioelement Mapping Using Gamma Ray Spectrometry Data. INTERNATIONAL ATOMIC ENERGY AGENCY, Vienna. https://www.iaea.org/publications/6746/guidelines-for-radioelement-mapping-using-gamma-ray-spectrometry-data, (accessed 16/04/2022).
Kareksela, S., Haapalehto, T., Juutinen, R., Matilainen, R., Tahvanainen, T., Kotiaho, J.S., 2015. Fighting carbon loss of degraded peatlands by jump-starting ecosystem functioning with ecological restoration. Sci. Total Environ. 537, 268–276. https://doi.org/10.1016/j.scitotenv.2015.07.094.
Kiely, G., Carton, O., 2010. SoilC - Measurement and Modelling of Soil Carbon Stocks and Stock Changes in Irish Soils, https://www.epa.ie/publications/research/land-use-soils-and-transport/soilc—measurement-and-modelling-of-soil-carbon-stocks-and-stock-changes-in-irish-soils.php, (accessed 09/05/2022).
Kosztra, B., Büttner, G., Hazeu, G., Arnold, S., 2017. Updated CLC illustrated nomenclature guidelines, European Topic Centre on Urban, land and soil systems (ETC/ULS). https://land.copernicus.eu/user-corner/technical-library/corine-land-cover-nomenclature-guidelines/docs/pdf/CLC2018_Nomenclature_illustrated_guide_20190510.pdf, (accessed 09/05/2022).
Martelet, G., Truffert, C., Tourliere, B., Ledru, P., Perrin, J., 2006. Classifying airborne radiometry data with Agglomerative Hierarchical Clustering: A tool for geological mapping in context of rainforest (French Guiana). Int. J. Appl. Earth Obs. Geoinf. 8 (3), 208–223. https://doi.org/10.1016/j.jag.2005.09.003.
McBratney, A.B., Santos, M.L.M., Minasny, B., 2003. On digital soil mapping. Geoderma 117 (1–2), 3–52. https://doi.org/10.1016/S0016-7061(03)00223-4.
Merchant, M.A., Adams, J.R., Berg, A.A., Baltzer, J.L., Quinton, W.L., Chasmer, L.E., 2017. Contributions of C-Band SAR Data and Polarimetric Decompositions to Subarctic Boreal Peatland Mapping. IEEE J. Sel. Top. Appl. Earth Obs. Remote Sens. 10 (4), 1467–1482. https://doi.org/10.1109/JSTARS.2016.2621043.
Minasny, B., Berglund, Ö., Connolly, J., Hedley, C., de Vries, F., Gimona, A., Kempen, B., Kidd, D., Lilja, H., Malone, B., McBratney, A., Roudier, P., O'Rourke, S., Rudiyanto, Padarian, J., Poggio, L., ten Caten, A., Thompson, D., Tuve, C., Widyatmanti, W., 2019. Digital mapping of peatlands - A critical review. Earth-Sci. Rev. 196, 102870. https://doi.org/10.1016/j.earscirev.2019.05.014.
Minty, B.R.S., 1997. Fundamentals of airborne gamma-ray spectrometry. accessed 09/05/2022 AGSO J. Aust. Geol. Geophys. 17 (2), 39–50. http://inis.iaea.org/search/search.aspx?orig_q=RN:28049082,.
Møller, M.F., 1993. A scaled conjugate gradient algorithm for fast supervised learning. Neural Networks 6 (4), 525–533. https://doi.org/10.1016/S0893-6080(05)80056-5.
Monteverde, S., Healy, M.G., O'Leary, D., Daly, E., Callery, O., 2022. Management and rehabilitation of peatlands: The role of water chemistry, hydrology, policy, and emerging monitoring methods to ensure informed decision making. Ecol. Inf. 69, 101638 https://doi.org/10.1016/j.ecoinf.2022.101638.
Novresiandi, D.A., Nagasawa, R., 2017. Polarimetric synthetic aperture radar application for tropical peatlands classification: a case study in Siak River Transect, Riau Province. Indonesia. J Appl Remote Sens 11 (1), 016040. https://doi.org/10.1117/1.JRS.11.016040.
Priori, S., Bianconi, N., Costantini, E.A.C., 2014. Can γ-radiometrics predict soil textural data and stoniness in different parent materials? A comparison of two machine-learning methods. Geoderma 226–227, 354–364. https://doi.org/10.1016/j.geoderma.2014.03.012.
Qiu, C., Zhu, D., Ciais, P., Guenet, B., Peng, S., Xu, X., 2020. The role of northern peatlands in the global carbon cycle for the 21st century. Glob. Ecol. Biogeogr. 29 (5), 956–973. https://doi.org/10.1111/geb.13081.
Rawlins, B.G., Lark, R.M., Webster, R., 2007. Understanding airborne radiometric survey signals across part of eastern England. Earth Surf. Proc. Land. 32 (10), 1503–1515. https://doi.org/10.1002/esp.1468.
Reinhardt, N., Herrmann, L., 2019. Gamma-ray spectrometry as versatile tool in soil science: A critical review. J. Plant Nutr. Soil Sci. 182 (1), 9–27. https://doi.org/10.1002/jpln.201700447.
Searchinger, T., James, O., Dumas, P., 2022. Europe's Land Future? Opportunities to use Europes land to fight climate change and improve biodiversity;and why proposed policies could undermine both, https://scholar.princeton.edu/tsearchi/publications/europes-land-future, (accessed 09/05/2022).
SGL, 2017. Fixed-Wing High-Resolution Aeromagnetic, Gamma-ray Spectrometric and Frequency-Domain Electromagnetic Survey. In: G.S.o. Ireland (Ed.), https://secure.dccae.gov.ie/GSI_DOWNLOAD/Tellus/SGL_Tech_Report_831A2_000.pdf, (accessed 09/05/2022).
Shen, C.P., 2018. A Transdisciplinary Review of Deep Learning Research and Its Relevance for Water Resources Scientists. Water Resour. Res. 54 (11), 8558–8593. https://doi.org/10.1029/2018WR022643.
Siemon, B., Ibs-von Seht, M., Frank, S., 2020. Airborne Electromagnetic and Radiometric Peat Thickness Mapping of a Bog in Northwest Germany (Ahlen-Falkenberger Moor). Remote Sens-Basel 12 (2). https://doi.org/10.3390/rs12020203.
Tanneberger, F., Tegetmeyer, C., Busse, S., Barthelmes, A., Shumka, S., Marine, A.M., Jenderedjian, K., Steiner, G.M., Essl, F., Etzold, J., Mendes, C., Kozulin, A., Frankard, P., Milanovic, D., Ganeva, A., Apostolova, I., Alegro, A., Delipetrou, P., Navratilova, J., Risager, M., Leivits, A., Fosaa, A.M., Tuominen, S., Muller, F., Bakuradze, T., Sommer, M., Christanis, K., Szurdoki, E., Oskarsson, H., Brink, S.H., Connolly, J., Bragazza, L., Martinelli, G., Aleksans, O., Priede, A., Sungaila, D., Melovski, L., Belous, T., Saveljic, D., de Vries, F., Moen, A., Dembek, W., Mateus, J., Hanganu, J., Sirin, A., Markina, A., Napreenko, M., Lazarevic, P., Stanova, V.S., Skoberne, P., Perez, P.H., Pontevedra-Pombal, X., Lonnstad, J., Kuchler, M., Wust-Galley, C., Kirca, S., Mykytiuk, O., Lindsay, R., Joosten, H., 2017. The peatland map of Europe. Mires Peat 19. https://doi.org/10.1111/rec.12865.
Treat, C.C., Kleinen, T., Broothaerts, N., Dalton, A.S., Dommain, R., Douglas, T.A., Drexler, J.Z., Finkelstein, S.A., Grosse, G., Hope, G., Hutchings, J., Jones, M.C., Kuhry, P., Lacourse, T., Lahteenoja, O., Loisel, J., Notebaert, B., Payne, R.J., Peteet, D.M., Sannel, A.B.K., Stelling, J.M., Strauss, J., Swindles, G.T., Talbot, J., Tarnocai, C., Verstraeten, G., Williams, C.J., Xia, Z.Y., Yu, Z.C., Valiranta, M., Hattestrand, M., Alexanderson, H., Brovkin, V., 2019. Widespread global peatland establishment and persistence over the last 130,000 y. P. Natl. Acad. Sci. USA 116 (11), 4822–4827. https://doi.org/10.1073/pnas.1813305116.
Valentine, A., Kalnins, L., 2016. An introduction to learning algorithms and potential applications in geomorphometry and Earth surface dynamics. Earth Surf. Dynam. 4 (2), 445–460. https://doi.org/10.5194/esurf-4-445-2016.
Vodyanitskii, Y.N., Grebenkin, N.A., Manakhov, D.V., Sashchenko, A.V., Tiuleneva, V.M., 2019. Positive Uranium Anomalies in the Peatlands of Humid Zone. A Review. Eurasian Soil Sci+ 52 (12), 1533–1541. https://doi.org/10.1134/S1064229319120135.
Wang, L., Qu, J.J., 2009. Satellite remote sensing applications for surface soil moisture monitoring: A review. Front Earth Sci. China 3 (2), 237–247. https://doi.org/10.1007/s11707-009-0023-7.
Wijedasa, L.S., Sloan, S., Michelakis, D.G., Clements, G.R., 2012. Overcoming Limitations with Landsat Imagery for Mapping of Peat Swamp Forests in Sundaland. Remote Sens-Basel 4 (9), 2595–2618. https://doi.org/10.3390/rs4092595.
Wilson, D., Blain, D., Couwenberg, J., Evans, C.D., Murdiyarso, D., Page, S.E., Renou-Wilson, F., Rieley, J.O., Sirin, A., Strack, M., Tuittila, E.S., 2016. Greenhouse gas

emission factors associated with rewetting of organic soils. Mires Peat 17. https://doi.org/10.19189/MaP.2016.OMB.222.
Xu, J.R., Morris, P.J., Liu, J.G., Holden, J., 2018. PEATMAP: Refining estimates of global peatland distribution based on a meta-analysis. Catena 160, 134–140. https://doi.org/10.1016/j.catena.2017.09.010.
Yu, Z., Loisel, J., Brosseau, D.P., Beilman, D.W., Hunt, S.J., 2010. Global peatland dynamics since the Last Glacial Maximum. Geophys. Res. Lett. 37 (13) https://doi.org/10.1029/2010GL043584.
Yu, Z., Beilman, D.W., Frolking, S., Macdonald, G.M., Roulet, N.T., Camill, P., Charman, D.J., 2011. Peatlands and Their Role in the Global Carbon Cycle. Eos, Trans. Am. Geophys. Union 92 (12), 97–98. https://doi.org/10.1029/2011EO120001.
Zhang, G.L., Liu, F., Song, X.D., 2017. Recent progress and future prospect of digital soil mapping: A review. J. Integr. Agr. 16 (12), 2871–2885. https://doi.org/10.1016/S2095-3119(17)61762-3.